Cellulose From Aloe Vera Plant Waste as Crosslinker for Vat 3D Printable Vitrimers: Toward a Circular Economy Approach in Additive Manufacturing

Macromolecular Materials and Engineering

Macromolecular Materials and Engineering Open Access

www.mame-journal.de

RESEARCH ARTICLE OPEN ACCESS

Cellulose From Aloe Vera Plant Waste as Crosslinker for Vat 3D Printable Vitrimers: Toward a Circular Economy Approach in Additive Manufacturing

Sara Bergia[1] | Maria Vittoria Piras[2] | Francesco Secci[2] | Guido Ennas[2] | Sara Paniziutti[2] | Francesca Frascella[2] | Alessandra Cabizza[3] | Ignazio Roppolo[1,4] | Annalisa Chiappone[2]

[1]Dipartimento di Scienza Applicata e Tecnologia, Politecnico di Torino, Turin, Italy | [2]Dipartimento di Scienze Chimiche e Geologiche, Università degli Studi di Cagliari, Complesso Universitario di Monserrato, Monserrato (Cagliari), Italy | [3]Lab7 Srl, Cagliari, Italy | [4]Center for Sustainable Future Technologies, Italian Institute of Technology, Turin, Italy

Correspondence: Ignazio Roppolo (ignazio.roppolo@polito.it)

Received: 21 September 2025 | **Revised:** 17 December 2025 | **Accepted:** 23 January 2026

Keywords: bio-based polymers | microcrystalline cellulose | photopolymerization | Vat printing | vitrimers

ABSTRACT

The reduction of the environmental impact of photocurable resins, commonly used in vat 3D printing, is an urgent request. In order to truly enable vat additive manufacturing (AM) to adopt a circular economy approach, this can be done by both selecting non-fossil carbon feedstocks and considering the end-of-life and reprocessability of the resulting thermosets. Pursuing this goal, we present the study of a 3D printing-compatible vitrimeric resin capable of dynamically reorganizing the polymeric network and exhibiting self-repair properties following heat treatment at 160°C. For the development of the resin, microcrystalline cellulose (MCC) is extracted from aloe vera peel, the main waste from the cultivation of this plant. MCC is then functionalized and used as an added-value crosslinker for the monofunctional monomer 2-hydroxy-3-phenoxypropyl acrylate (HPPA), which is considered green as it can be obtained from renewable resources. The material studied possesses excellent printing resolution, remodeling, and self-healing ability, leading to a significant recovery of mechanical properties after breakage. This work highlights the possibility of combining renewable raw materials, waste utilization, and vitrimeric chemistry to create sustainable, easily recyclable resins.

1 | Introduction

Additive manufacturing (AM), also referred to as 3D printing, has assumed a key role in the recent industrial revolution known as Industry 4.0 [1], as it allows the manufacture of 3D objects with complex geometries without the use of molds, dies or lithographic masks. [2] Furthermore, it is not only limited to prototypes, but is also used as small-scale production because it is cheap, versatile in the materials that can be made and allows for high customization [3], making it ideal for various industries such as aerospace, automotive and healthcare [4–8].

Among the various AM techniques, vat 3D printing uses light to light-cure photosensitive resins layer by layer. One of the most popular vat technologies is digital light processing (DLP) in which the light projector uses a high-power LED source, and it is based on a micro-electromechanical system (MEMS) that uses a digital mirror device (DMD) to project the desired light patterns [9].

This technique has numerous advantages, including fast printing, high resolution of printed objects, which can reach a minimum of 50 μm [10], and a significant reduction in costs and material

TABLE 1 | Summarized composition of the vitrimeric formulations.

Resin	HPPA wt.%	GDGDA wt.%	MCC wt.%	Miramer A99 wt.%	BAPO phr
HG10	75	10	\	15	2
HC5	80	\	5	15	2
HC10	75	\	10	15	2
HC15	70	\	15	15	2

waste, as it uses less energy and space, making it a more sustainable option than conventional production methods [11].

Due to intrinsic characteristics of DLP, most of the materials produced are thermosets, which usually have well-known advantages such as good mechanical and thermal properties, dimensional stability, and chemical resistance, due to the irreversible cross-linking covalent bonds [12]. On the other hand, these permanent cross-linking points have some drawbacks, among which the most relevant are the poor possibility to be repaired and recycled. In this context, 90% of thermosets are incinerated or landfilled [13] at the end of their use, creating major sustainability problems [14]. Furthermore, the DLP resins currently on the market are usually based on acrylates and/or epoxides of synthetic origin, derived from fossil resources with a high carbon footprint [15, 16].

To reduce the environmental impact, it is therefore essential to begin a transition to more environmentally friendly resins, which are based on ingredients from bioresources and, at the same time, are easier to recycle [17]. This would promote a circular economy, reduce waste, and decrease pollution [18]. To this purpose, in the latest years vitrimers emerged as a valuable option. Those are polymers with covalent adaptable networks (CAN) that are able to reorganize their topology under the influence of external stimuli such as light, heat or catalysts [19, 20].

The behavior of the temperature-dependent materials is closely related to the topological freezing transition temperature (T_v), usually defined at the point where the material reaches a viscosity of 10^{12} Pa·s [21]. At temperatures below T_v, vitrimers behave like traditional thermosets, maintaining excellent mechanical properties. However, above this temperature, dynamic bond exchange reactions are triggered, which allow an increase in segmental mobility without compromising the material structure [22]. Above T_v, vitrimers acquire new properties, such as healing ability, malleability, reprocessability and recyclability, ideal for more sustainable materials. [23] Over time, various dynamic exchange reactions have been studied, including transesterification, transamination, transcarbamoylation, disulfide exchange, imine exchange, and many others [24]. Among these, transesterification mechanisms have attracted particular interest due to their simplicity in synthesis and suitability for a wide range of monomers. [25–28] Biobased vitrimers were recently studied to develop 3D printable formulations that combine sustainability and reworkability. For instance, systems based on lignin, vanillin and soybean oil have demonstrated self-healing properties through transesterification and good mechanical performance, with a biobased content of up to 70 wt.% [29]. More recently, UV-polymerisable vitrimeric resins composed of glycerol, soybean oil and tetrahydrofurfurylmethacrylate derived from hemicellulose have been successfully applied in DLP 3D printing, showing excellent reworkability, shape memory and repairability capabilities. [30] In another study, bis-dynamic networks obtained from vanillin and cystamine, containing disulphide and imine bonds, led to the development of printable resins with self-healing and shape memory properties at both room-temperature and elevated temperatures, as well as the possibility of re-printing after chemical recovery, expanding the circular potential of these materials [31].

Rooted on these approaches, the present work focuses on the use of upcycled waste from local mediterranean cultivation, aiming to enter the mindset of circular economy also when talking about DLP printable resins. Complex, high-resolution parts were printed using vitrimeric formulations based on microcrystalline cellulose (MCC) extracted from Aloe Vera peels which are, a by-product of the cosmetics industry. The cellulose was functionalized to obtain a light-curable methacrylate derivative to be used as a hydroxyl-rich crosslinker in the development of a dynamic network able to undergo transesterification reactions.

2 | Materials and Methods

2.1 | Materials

Dimethylformamide (DMF), methacrylic anhydride, Sodium Hydroxide (NaOH), Sufuric acid, Ethanol, 2-Hydroxy-3-phenoxypropyl acrylate (HPPA), Glycerol 1,3-diglycerolate diacrylate (GDGDA) and Phenylbis (2,4,6-trimethylbenzoyl) phosphine oxide (BAPO) were purchased from Merck Sigma–Aldrich. Miramer A99, methacrylate phosphate, was purchased from Miwon Europe GmbH. Aloe Vera Peels were supplied by Lab 7 s.r.l. Cagliari (CA). The monomers used are sketched in Figure S1.

2.2 | MCC Extraction and Functionalization

MCC was extracted from aloe peels with small modifications to previously reported methods [32]. Briefly, Aloe Vera peels were cut into pieces (ca. 2 × 2 mm^2), liophylized and grinded to produce homogeneous powders with a diameter of about 200 μm. The powder was then subjected to Soxhlet extraction using ethanol for 24 h. Subsequently, the powder (~15 g) was subjected solvothermal hydrolysis. This process was performed in an autoclave (Teflon autoclave with a steel jacket, 300 mL) using

a 1:1 H_2O-EtOH mixture (90 mL) in the presence of sulfuric acid (0.05 M) at 150°C for 6 h. After returning to room-temperature, the solid was filtered and washed with hot distilled water. The filtered solid was then dried under an IR lamp for 2 h. Subsequently, a bleaching step was followed: a 7.5% w/v solution of H_2O_2 (at 30% v/v) and 5% w/v of NaOH was prepared. The bleaching was carried out under reflux for 2 h at 75°C with vigorous stirring. Once brought to room-temperature, the mixture was filtered, washed with hot distilled water, and subjected to treatment in an ultrasonic bath with abundant water. The purification process was repeated until a neutral pH was reached. The solid was dried in an oven at 100°C to evaporate water and impurities. The process was repeated four times. Then, the obtained powder was suspended in an aqueous solution of 6% HCl and stirred at 80°C for 1 h. After that, the suspension was neutralized by adding dropwise an aqueous solution of NaOH until pH 7 was reached. The resulting media was left to rest for 10 h at room-temperature to allow Cellulose precipitation. The cellulose-based powder was filtered and washed with ethanol and dried under vacuum at 60°C for 10 h.

For the preparation of methacrylated MCC, cellulose, dimethylformamide (DMF), and methacrylic anhydride were used in respective weight ratios of 20:40:40. The resulting solution was left overnight at 70°C under a fume hood. Subsequently, the acrylate cellulose was washed three times with EtOH, filtered through a Buchner funnel, and allowed to dry at 40°C overnight under vacuum conditions. The resulting powder was subjected to dialysis against distilled water for 3 days.

2.3 | Preparation of the Formulations

Four light-curable formulations were prepared with different weight ratios between the functional monomer and the crosslinker, while the weight of the catalyst Miramer A99 remained unchanged, according to previous studies [33]. The formulations were thoroughly mixed by magnetic stirring until a homogeneous resin was obtained. Then 2 phr (per hundred resin) of BAPO photoinitiator was added to each formulation and mixed again for 5 min at room-temperature. The composition of the acrylic resin formulations is summarized in Table 1.

Each solution was prepared in a black flask to prevent premature photopolymerization of the resin due to visible light.

2.4 | 3D printing

A DLP-3D printer (Asiga MAX X27 UV, Australia) was used for printing. The light source of the printer was based on LEDs that emit at 385 nm, and the system offers a nominal resolution of 50 μm in the XY plane and 1 μm along the *Z* axis. The structures were 3D printed by setting a printing slicing thickness of 50 μm and a light intensity of 35 mW cm^{-2}. All CAD designs were created with the SolidWorks program and exported in STL format to be used in the Asiga Composer software.

The printed parts were washed with acetone and then subjected to a post-curing treatment in a UV oven (Asiga Flash) to complete the cross-linking (3 min on each side).

2.5 | Characterization Technique

X-ray analysis. XRPD patterns of the cellulose powder were recorded with Cu–Kα radiation (λ = 1.54056 Å) using a Seifert x3000TT Diffractometer in the Bragg–Brentano geometry with a step size of 0.05 2θ° in an angle range 4° ≤ 2θ ≤ 50° An appropriate acquisition time was selected to obtain a satisfactory signal-to-noise ratio. Based on the relative intensities of the crystalline peaks compared to the amorphous contribution—considered at the minimum point between the peaks in the X-ray diffraction pattern—it is possible to estimate the crystallinity index (CI) of the sample using the following formula:

$$CI\ \% = \left(1 - \frac{I_A}{I_{200}}\right) \times 100$$

where I_A the intensity of the amorphous region and I_{200} is the intensity of the crystalline peak.

^{13}C CP/MAS NMR: spectra were recorded on a Bruker Avance III HD at 5 kHz rotation, contact time: 2 ms, delay: 3, line broadening: 10 Hz.

For the acrylated portion, the characteristic signals were considered:

The methyl carbons (CH3), located around 20 ppm, correspond to one carbon per acrylate group; the vinylic carbons (C═C), between 135 and 125 ppm, correspond to two carbons per acrylate group.

The degree of substitution (DS) was calculated using the following formula:

$$DS = [\ (I_A/n_{C,A})/\ (I_{c1}/N_{c1})]$$

Where:

I_A is the integral of the selected acrylate group signals, $n_{C,A}$ is the number of carbons represented by that signal (2 for C═C, 1 for CH_3), I_{C1} is the integral of the anomeric carbon signal, n_{C1} = 1.

Photoreology tests were conducted on liquid formulations to study the kinetics of polymerization using a Hamamatsu LC8 broad-spectrum UV lamp and an Anton Paar MCR 302 rheometer with a coupled flat-plate configuration (frequency 1 Hz, amplitude of oscillation 1%).

Rheological tests were performed on liquid formulations to observe changes in viscosity as a function of strain rate (γ') using an Anton Paar MCR 302 rheometer with a parallel plate configuration.

Stress relaxation tests were conducted to verify that the formulations followed vitrimeric behavior. an Anton Paar MCR 302 rheometer with a parallel plate configuration was used. Samples were preloaded with a force of 10 N for 5 min at the set temperatures of 140°C, 150°C, 160°C, 165°C and 170°C, then a strain of 10% was applied and the relaxation modulus was measured.

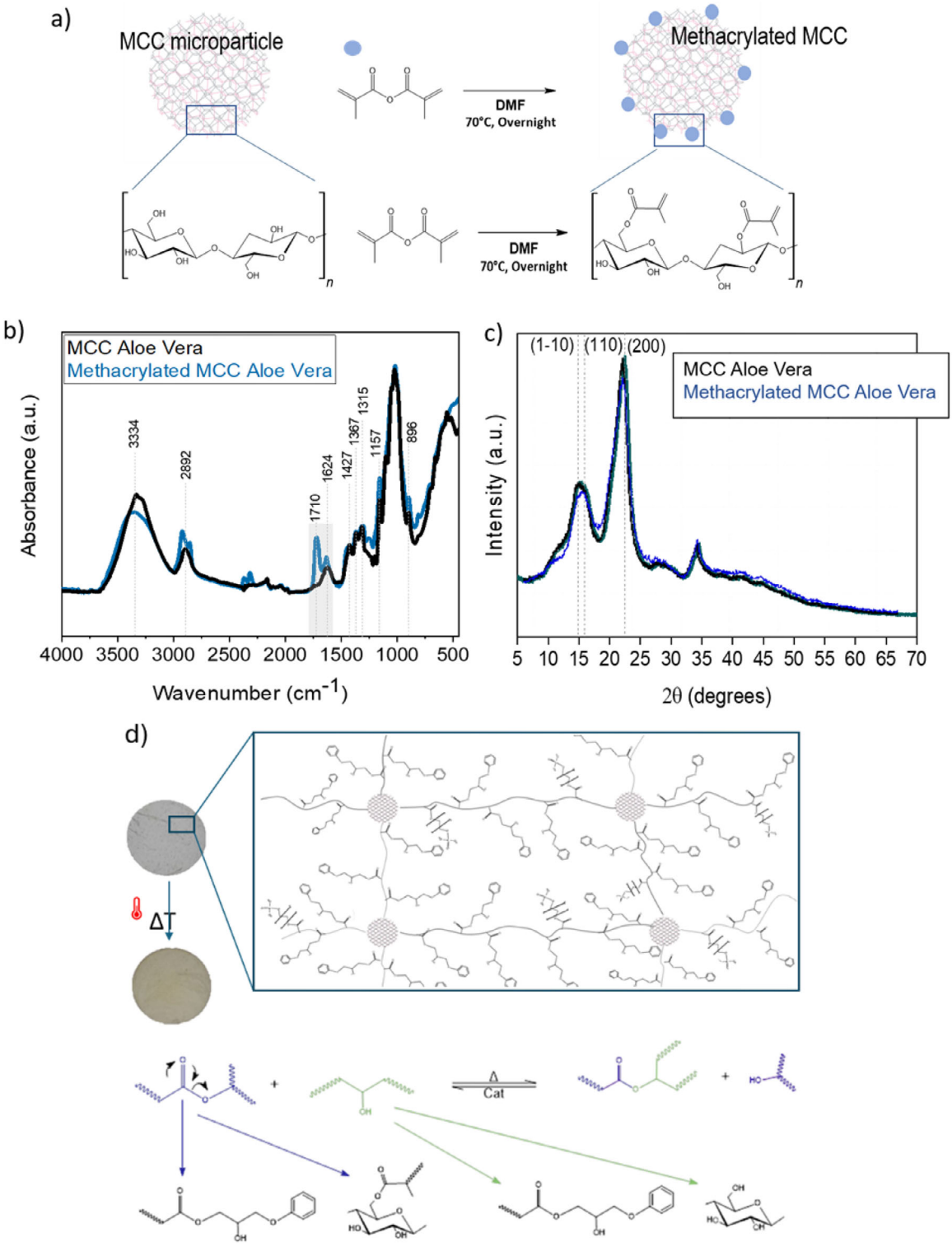

FIGURE 1 | a) Scheme depicting the MCC methacrylation process; b) FT-IR of the extracted MCC compared with the same after the methacylation process; c) XRPD of the extracted MCC compared with the same after the methacylation process; d) scheme of the polymer network and of the transesterification mechanism.

Morphology Field emission scanning electron microscope (FESEM, Zeiss Supra 40) has been used to investigate the dispersion and distribution of MCC. Cross section images were taken from specimens after tensile testing. For comparisons MCC powder was analyzed. All the sample were observed after metallization.

Gel Content tests were conducted to obtain an indication of the amount of unreacted monomer at the end of the polymerisation process. The samples were initially weighed, immersed for 24 h in acetone, and then reweighed after drying for 48 h to allow the solvent to evaporate. The gel content was calculated gravimetrically as the ratio of the weights after and before

extraction. The measurements were repeated three times, and the results averaged.

Swelling tests were conducted to measure the absorption and deformation capabilities of the material. the samples were weighed initially when dry and then immersed in acetone and reweighed in precise time steps until a plateau was reached.

Fourier Transform Infrared Spectroscopy (FT-IR). Attenuated total reflection (ATR) spectra were collected using a Thermo Scientific Nicolet iS50 FTIR spectrometer. 64 scans were collected for each sample in the range of 4000–500 cm^{-1}, with a resolution of 2 cm^{-1}. The graphs obtained were normalized with respect to the peak at 1720 cm^{-1} corresponding to the vibration of the carbonyl groups to improve comparisons between the different spectra.

DSC (Differential Scanning Calorimetry) analyses were conducted to study the thermal properties of formulations with a DSC 204 F1 Phoenix machine used in an air atmosphere. In the heating phases, the temperature was increased from 0°C to 180°C at a rate of 5°C/min, while in the cooling phases, the temperature was lowered from 180°C to 0°C at a rate of 20°C/min. Between cycles, 30 min isotherms were set to reach the desired final temperatures.

Thermogravimetric coupled infrared absorption analyses (TGA-IR) were conducted using a NETZSCH TG 209 F1 Thermogravimetric Analyzer coupled by a transfer line heated at 230°C with an infrared spectrometer Bruker TENSOR II equipped with an IR gas cell heated at 200°C. The tests were performed in alumina pans with nitrogen flux of 20 mL min^{-1} and heating from 20 to 180°C at a rate of 10 K min^{-1} for about 10 mg of sample. Three vacuum cycles were performed before the test. The FTIR analysis was collected in the absorbance mode in the range 650–4400 cm^{-1}. Standard TGA experiments were also performed in the range 25–800°C in air (flux 50 mL/min) with a heating rate of 10°C.

3D scanner was used to compare the printed geometry with that obtained with CAD software, and thus be able to evaluate the printing fidelity. The scanner used was the 3Shape E4 (3Shape A/S, Copenhagen, Denmark), with a measurement accuracy of 4 µm.

Self-healing characterization procedure: For the self-healing experiments, reference specimens (dumbbell specimens with an effective cross-section of 17 × 6 × 2 mm), and broken specimens prepared with a hole in their main body and the corresponding disk (3.5 mm diameter) were produced by DLP 3D printing. A MEMMERT vacuum oven at 160°C for 4 h was used for heat treatment.

Tensile tests were conducted to determine the elastic modulus value using an Instron machine with a load cell capacity of 500 N for the material before heat treatment and 10 kN for the heat-treated material, with a strain rate of 10 mm/min.

Recyclability tests Procedure: Experimental tests were conducted to verify the ability to recycle by creating thin films (900 µm films) from material's fragments pressed at 160°C with a pressure of 5 tons for 1 h and then performing tensile tests on the so-obtained specimens.

3 | Results and Discussion

The initial step of the work involved the extraction of cellulose from Aloe Vera cultivation waste and its functionalization (Figure 1a). Microcrystalline cellulose was obtained by combining a Soxhlet extraction and solvothermal method followed by alkaline bleaching and hydrolysis; the sequence of steps allowed to separate the different components of the natural waste: fatty acids and small molecules (e.g. antraquinones), lignin and hemicellulose from cellulose [32]. FT-IR analyses in ATR mode allowed to follow the modification of the biomaterial after each step, the obtained spectra are reported and commented in (Figure S2). The spectrum of the final product is reported in Figure 1b and shows the characteristic peaks of the cellulose structure. Specifically, the absorption peak at 896 cm^{-1} is associated with the asymmetric γCOC at β-glycosidic bond in the amorphous region, the peak centered at 1030 cm^{-1} corresponds to γCO asymmetric deformation at C6, the absorption band at 1157 cm^{-1} can be attributed to the γCOC at β-glycosidic linkage while the absorption peaks in the region from 1670 to 1315 cm^{-1} can be attributed to the vibration of the δCH_2 and δCOH and CH in the cellulose backbone [34]. The presence of a peak at 1624 cm^{-1} may be due to the bending of −OH groups from residual absorbed water. The broad peak at higher wavenumbers (3300 cm^{-1}) is instead related to the cellulose hydroxyl groups [35–38].

To further confirm the successful extraction of cellulose in its microcrystalline form, the XRPD pattern of the extracted powder has been collected (Figure 1c), resulting in the characteristic cellulose type I diffractogram with high width at half maximum, indicating the presence of nanocrystalline domains [39]. The diffraction peak (200) around 22.5° is due to the presence of the crystalline monoclinic lattice typical of native cellulose Iβ. While the region between this diffraction peak and the peak at 16° can be considered as consisting solely of an amorphous contribution [36]. The XRPD data analysis revealed a crystallinity index of 81%.

After the extraction procedure, the surface of the resulting MCC was functionalized with methacrylic moieties (Figure 1a); the effective grafting was confirmed after strong washing and dialysis by FT-IR. The presence of the peak centered at 1710 cm^{-1}, related to the presence of the carbonyl group, confirmed the successful reaction (Figure 1b, light green). The reduction of the intensity of the broad peak at higher wavenumbers (about 3300 cm^{-1}) further confirms the substitution of the –OH groups with the methacrylic moieties. 13C solid-state NMR was also performed (Figure S3), confirming the presence of double bonds on the surface of MCC microparticles; A degree of substitution (DS) of 0.075 was calculated from this analysis. Noteworthy, cellulose crystallinity was not influenced by the methacrylation process, as evidenced by the comparison of the XRPD spectra of MCC before and after functionalization, reported in Figure 1c, indeed DMF is a solvent that does not disrupt the cellulose intermolecular structure, maintaining the semicrystalline nature of the microparticles.

Then, vitrimeric DLP-printable formulations were developed. A formulation described elsewhere [33] based on synthetic polymers, and already demonstrated to be suitable for fabricating 3D printable vitrimers, was chosen as reference. This material is based on HPPA, which is a non-toxic, biodegradable monomer,

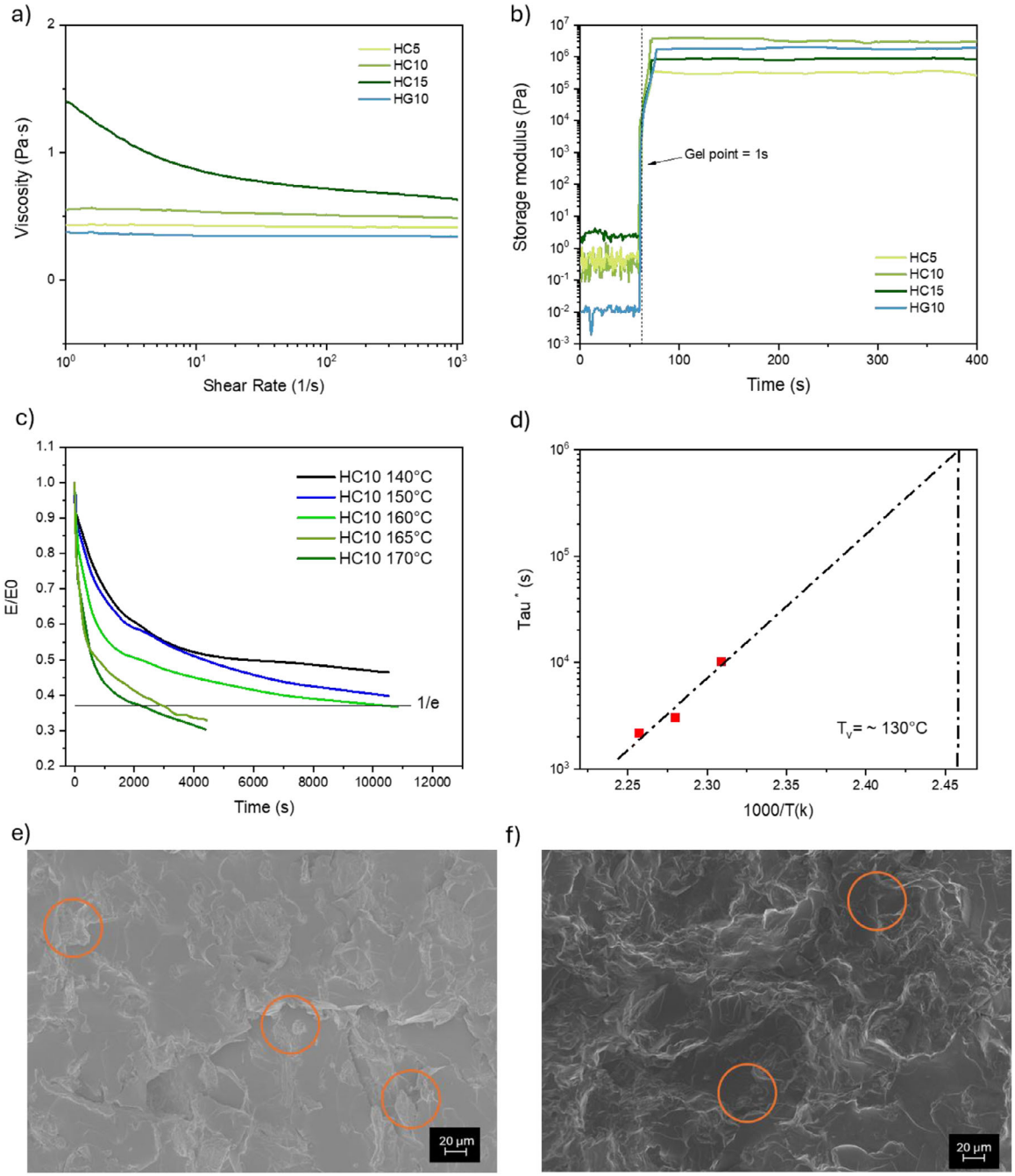

FIGURE 2 | a) photoreology test; b) rheology test; c) stress relaxation test on HC10 at different temperatures; d) Arrhenius plot obtained from stress relaxation tests on HC10; e) SEM image of printed HC10 at 1KX magnification; f) SEM image of HC10 after heat treatment at 1KX magnification. Circle are intended to show MCCs crystals, so that they can be distinguished in the polymeric matrix.

and is considered a green material because it can be produced from renewable resources [30]. The previously studied formulation used GDGA as a synthetic crosslinker that was here replaced with increasing amounts of the methacrylated MCC obtained from plant waste, to develop a more sustainable vitrimeric resin for 3D printing. A scheme of the polymeric network and of the mechanisms envisaged in this work is reported in Figure 1d. Rheological measurements were performed to analyze the viscosity behavior in the range of interest of the DLP printer (1 to 10 1/s). All resins showed linear behavior, except for the 15% MCC formulation, which showed non-linearity problems in the range of interest, probably due to the formation of MCC aggregates in the resin (Figure 2a). This increase of viscosity is typical of composite materials and reflects the reduced mobility of polymeric chains due to the presence of an increasing amount of MCC in the formulations.

Afterward, photoreology tests were conducted to assess the kinetics of polymerization. The results showed that all biobased formulations exhibited similar behavior to the reference formulation containing the synthetic crosslinker, reaching gel point within one second of UV lamp activation. Despite similar gel

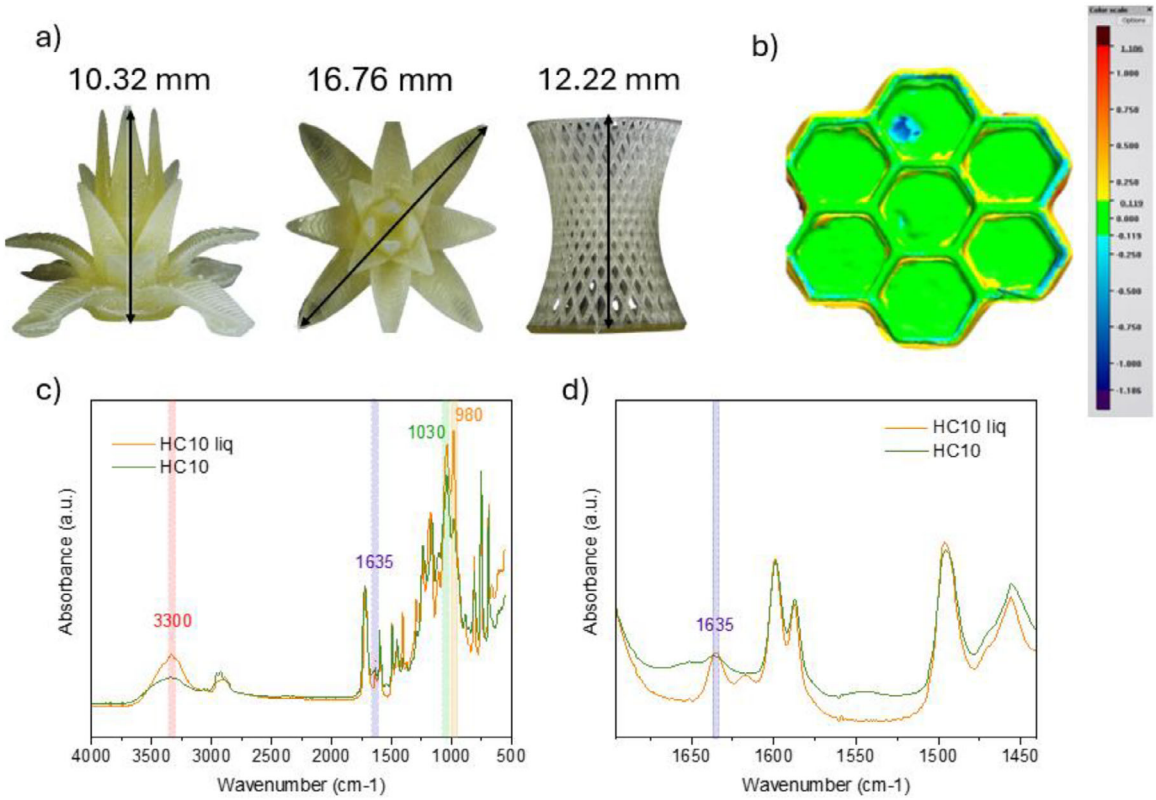

FIGURE 3 | a) examples of HC10 printed objects with complex geometries; b) 3D scanner of honeycomb printed with HC10 resin; c) ATR spectra comparison before and after phototopolymerization process, evidencing the peaks of interest; d) decrease of methacrylate peak at 1635 revealed by ATR spectroscopy.

times, the final storage modulus showed differences between formulations, consistent with the effect of MCC steric hindrance on network formation. In particular, the formulations the formulation HC10 showed the highest mechanical properties, even higher than the counterpart with synthetic crosslinker (HG10) (Figure 2b). A further decrease of MCC instead leads to worse mechanical properties, probably due to the higher viscosity which hinders the network formation. Based on these experiments, formulations HC15 and HC5 were excluded from subsequent investigations because for the purpose of the work, it is useful to have the highest possible weight percentage of cellulose without compromising the viscosity of the resin. Therefore, HC10 was chosen as the final formulation for comparison with the synthetic vitrimer HG10.

To verify that the vitrimeric properties were maintained even with the replacement of the crosslinker, disc specimens were fabricated using the DLP technique, and stress relaxation tests were conducted on these by pre-heating the discs at different temperatures, ranging from 140°C to 170°C (Figure 2c). The HC10 material showed behavior following the trend modeled by the Maxwell equation, reaching the horizontal asymptote of 1/e at 160°C.

The stress relaxation tests were then used to derive the Arrhenius plot, with a topology freezing temperature T_v of 130°C (Figure 2d).

These results indicates that the use of the MCC crosslinker leads to stress relaxation behavior similar to that observed for the synthetic crosslinker (Figure S4). It can be speculated that, despite the functionalization with methacrylic moieties, the cellulose microparticles still present –OH rich surfaces that enhance dynamic bond exchange reaction (Figure 1d). The morphology of the obtained composite materials was investigated with FESEM, evidencing that MCC are crystals in the micrometric range (Figure S5a); the same morphology was preserved in the polymerized sample (Figure 2e), even after thermal process (Figure 2f). Furthermore, MCC resulted well distributed over the in the polymeric network (Figure S5b,c)

Once the vitrimeric behavior of the bio-based HC10 formulation had been confirmed, complex geometries were printed to assess its printability (Figure 3a). The printing allowed details down to 60 μm to be reproduced, highlighting the high-resolution of the system. Accuracy was verified by 3D scanning of a honeycomb structure (Figure 3b), chosen for its regular and symmetrical geometry, ideal for assessing dimensional fidelity in the XY plane. The deviation map shows a high degree of correspondence between the digital model and the printed object, with sharp edges, no visible distortions and dimensional errors contained within 100 μm. The slight local deviations observed are attributable to internal stress build-up or light scattering at the edges, phenomena typical of DLP printing that do not compromise overall dimensional reliability [40].

The optimized printing parameters are shown in Table 2. It is worthy to highlight that the printing process is fast with an average object production speed of 1 mm/min, thanks to the

TABLE 2 | printing parameters for HG10 and HC10.

HG10 and HC10	Burn-in (first 3 layers)	Other layers
Slice Thickness (mm)	0.07	0.1
Light Intensity (mW/cm^2)	35	35
Exposure time (s)	2	1
Temperature (°C)	30	30

combination of short irradiation times and minimal waiting intervals between layers, while maintaining high resolution.

In order to confirm the successful light-curing of the resin, solvent extraction tests and ATR analyses were performed. The %gel measurements provided a quantitative assessment of the insoluble fraction, indicating the formation of a stable polymer network at 96.7 ± 0,6% (Figure S6).

To complement this, ATR spectroscopy Was used to determine the conversion degree, monitoring the decrease of the characteristic C=C stretching peak to 1635 cm^{-1} [41], which directly reflects the progression of the polymerisation reaction (Figure 3c,d). Other peaks observed in the ATR spectra include a band at 980 cm^{-1}, attributed to the vibrations of the phosphate group (PO_4) of the catalyst [42], and the already discussed cellulose signals at 1030 cm^{-1}, and the broad hydroxyl groups (–OH) peak at 3300 cm^{-1}. These hydroxyl groups are crucial in the formulation, as they may promote the transesterification reaction (Figures S7 and S8). The thermal properties of the 3D printed samples were also evaluated by DSC (Figure S9). Thermograms show that pure HPPA has a glass transition temperature (T_g) around 26°C (Figure S9a). When MCC are added in the formulation (without Miramer catalyst), a broad exothermic peak appears in the first heating cycle at temperatures higher than 125°C, which can be related to residual polymerization, in fact the second heating cycle shows a T_g again at 26°C as neat HPPA and no other exothermic peaks (Figure S9b). Conversely, when the catalyst is added a sharper peak emerge, centred around 150°C and in the second cycle the T_g shifts to temperatures higher than 40°C (Figure S9c) indicating a rearrangement of the network. It can be argued that this peak is related to degradation, therefore TGA measurement was performed (Figure S9d), that indicates that the onset of degradation for HC10 is around 200°C.

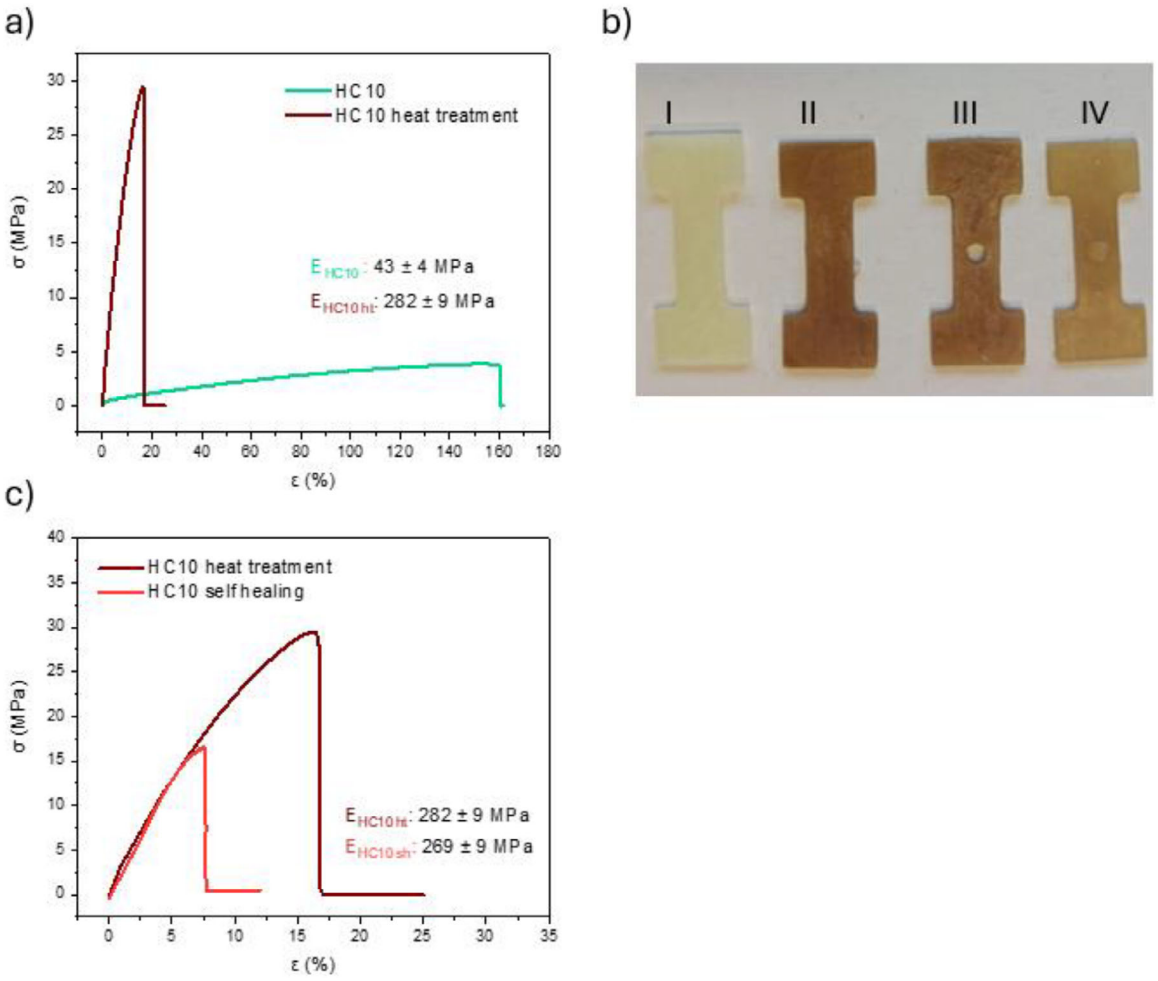

FIGURE 4 | a) tensile tests on HC10 before and after heat treatment at 160°C for 4 h; b) picture of sample HC10, printed (I), after the first heat treatment (II), after the first heat treatment with hole (III) and after the first heat treatment with hole repaired (IV); c) tensile testing on samples repaired by heat treatment.

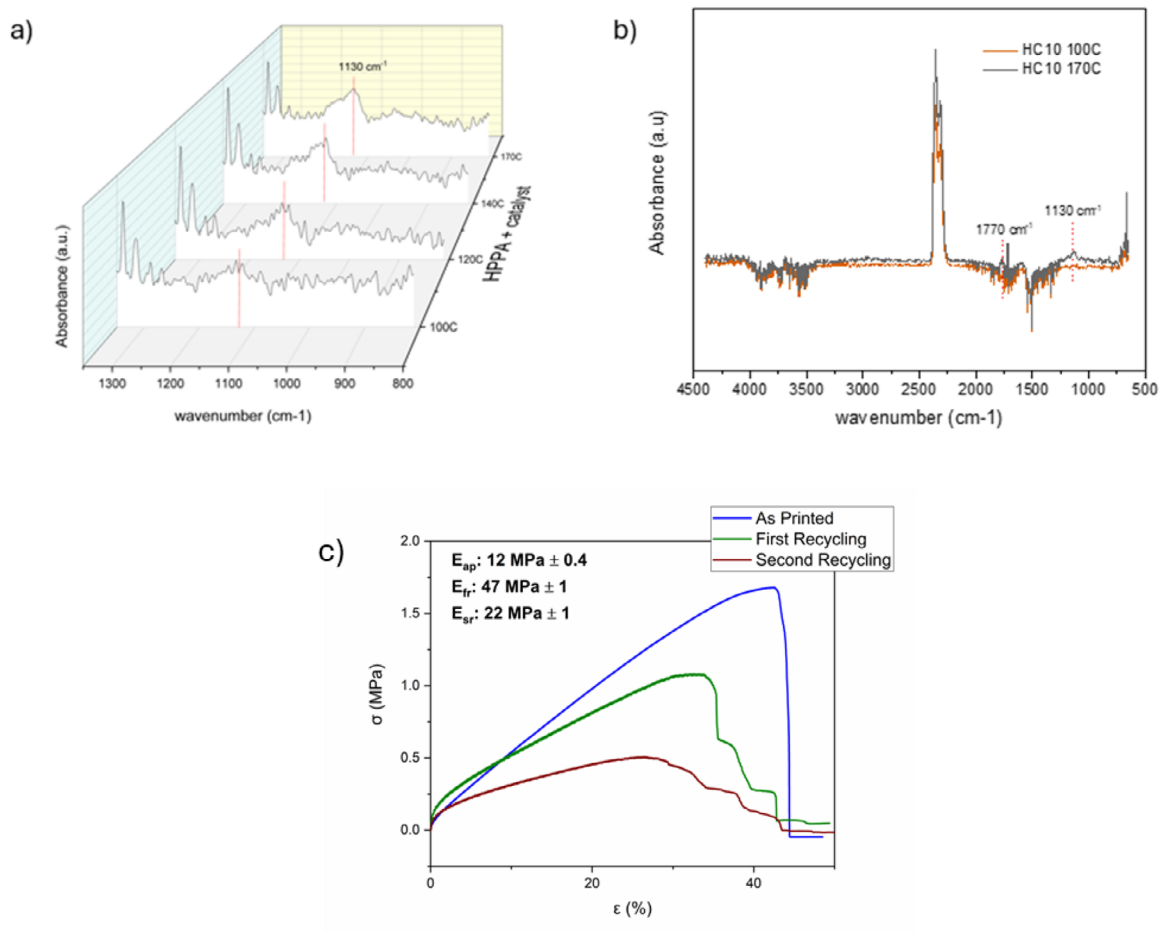

FIGURE 5 | a) TGA-IR analysis of HPPA + catalyst with peak formation at 1130 cm^{-1} with increasing temperature; b) TGA-IR analysis of HC10, with evidence of peaks at 1130 and 1770 cm^{-1} in the sample heated at 170°C; c) tensile test on thin films of HC10, printed, after the first thermal process and after the second thermal process.

Subsequently, the mechanical properties of the studied materials were investigated by means of uniaxial tensile tests; dumbbell shaped samples were printed, and the samples were submitted to a thermal heating 160°C for 4 h. Heating is essential to promote transesterification reactions and to allow the dynamic rearrangement of the network. After the heating treatment, the vitrimer shows a change in mechanical behavior: the elastic modulus increases from 43 ± 4 MPa with an elongation at break of 160%, to 282 ± 9 MPa with an elongation of 17% (Figure 4a). This transition reflects the change from a soft material to a much more rigid and brittle structure due to the densification of the network and further cross-linking, in agreement with DSC measurements. The occurrence of the transesterification reaction is expected to impart self-healing properties to the material; to evaluate this, printed specimens were drilled, the corresponding discs were reinserted and the material was heat-treated. After the healing process, approximately 95.4% of the original elastic modulus was recovered compared to the pristine samples, measuring an elastic modulus of 269 ± 9 MPa (Figure 4c,d).

Heat treatment triggered chemical transformations, [43] as revealed by TGA-IR analysis. Heating the HPPA alone did not produce significant spectral changes between 100°C and 170°C. (Figure S10a). However, in the presence of the catalyst that enabled transesterification, a new IR band appeared at 1130 cm^{-1}, attributed to the release of secondary alcohols during transesterification (Figure 5a). An additional band at 1770 cm^{-1} was observed in the complete HC10 formulation (Figure 5b, Figure S10b). Both bands can be attributed to the formation of volatile carbonyl-containing species, such as phenyl glycols. This was consistent with previous literature [44], which demonstrated the release of these species in this temperature range in synthetic polymers. Observing in detail TGA curves in the range below 180°C it is possible to observe a slight mass decrease (around 3%) which is in good agreement with spectroscopic measurements (Figure S10c). Noteworthy, this mass loss decreases after the thermal treatment, suggesting that the network is stabilized. On the other hand, observing the general degradation behavior, the 3D printed sample and the one subjected to thermal treatment have very similar thermograms, indicating that, although rearranged, the polymeric network was not totally modified (Figure S10d).

Finally, the recycling properties after multiple thermal processes were tested, performing tensile tests on films obtained by hot pressing of broken pieces of material (Figure 5c). In this case, the mechanical properties of the reprocessed materials are preserved. Interestingly, although a certain increase of E was measured after hot pressing, this is lower than the values measured in the case of simple thermal treatment and self-healing (Figure 4). In this case, it must be considered that the hot pressing has also a pressure

component (5 tons) that can modify the final materials properties. Related to maximum stress, this decrease in the processes, but this can also be related to defects induced by the procedure of fabrication of the specimens.

4 | Conclusion

In this work, a 2-hydroxy-3-phenoxypropyl acrylate-based vitrimeric resin was developed using methacrylate cellulose (MCC), derived from agricultural waste, as a bio-based crosslinker. The optimized formulation, containing 10% MCC by weight, showed excellent printability via DLP 3D printing technology, achieving resolutions of 60 μm, and precision below 100 μm, with extremely fast light-cure times. The tests performed confirmed the formation of a stable and dynamic polymer network, capable of activating transesterification reactions that allow the network to reorganize and the material to repair itself. Following heat treatment at 160°C, the material showed a marked increase in structural rigidity and the ability to recover up to 95% of the original elastic modulus after damage. Moreover, already at lower temperatures, it was possible to achieve material recycling through hot pressing. These characteristics highlight the real possibility of integrating advanced functionalities, such as self-repair and recycling, into 3D printing-compatible bio-based photopolymer resins, paving the way for new sustainable applications.

Acknowledgements

The authors want to thank Dr. Cecilia Mosino and Dr. Matteo Salvatore Uccheddu for their help in the improvement of the MCC extraction protocol. A.C. acknowledges the funding support from the European Union – Next Generation EU, component M4C2, investimento 1.1. PRIN 2022 PNRR Project "3D VOCe" code P2022JWF3P. This work was developed in the frame of VIVA3D research project, funded by Ministry of Ecological Transition (MITE).

Conflicts of Interest

The authors declare no conflict of interest.

Data Availability Statement

The data that support the findings of this study are available in the supplementary material of this article.

References

1. A. Jandyal, I. Chaturvedi, I. Wazir, A. Raina, and M. I. Ul Haq, "3D printing—A Review of Processes, Materials and Applications in Industry 4.0," *Sustainable Operations and Computers* 3 (2022): 33–42, https://doi.org/10.1016/j.susoc.2021.09.004.

2. L. Zhou, J. Miller, J. Vezza, M. Mayster, and M. Raffay, "Additive Manufacturing: A Comprehensive Review," *Sensors* 24, no. 9 (2024): 2668, https://doi.org/10.3390/s24092668.

3. J. Nam and M. Kim, "Advances in Materials and Technologies for Digital Light Processing 3D Printing," *Nano Convergence* 11, no. 45 (2024): 45, https://doi.org/10.1186/s40580-024-00452-3.

4. C. Radhika, R. Shanmugam, M. Ramoni, and G. Bk, "A Review on Additive Manufacturing for Aerospace Application," *Materials Research Express* 11, no. 2 (2024): 022001, https://doi.org/10.1088/2053-1591/ad21ad.

5. P. C. Priarone, A. R. Catalano, and L. Settineri, "Additive Manufacturing for the Automotive Industry: On the Life-cycle Environmental Implications of Material Substitution and Lightweighting Through Re-Design," *Progress in Additive Manufacturing* 8, no. 6 (2023): 1229–1240, https://doi.org/10.1007/s40964-023-00395-x.

6. E. R. Ghomi, F. Khosravi, R. E. Neisiany, S. Singh, and S. Ramakrishna, "Future of Additive Manufacturing in Healthcare," *Current Opinion in Biomedical Engineering* 17 (2021): 100255, https://doi.org/10.1016/j.cobme.2020.100255.

7. A. B. Singh, "Transforming Healthcare: A Review of Additive Manufacturing Applications in the Healthcare Sector," in *2nd Int. Electronic Conf. on Machines and Applications* (MDPI, 2024), https://doi.org/10.3390/engproc2024072002.

8. G. Palmara, F. Frascella, I. Roppolo, A. Chiappone, and A. Chiadò, "Functional 3D Printing: Approaches and Bioapplications," *Biosensors and Bioelectronics* 175 (2021): 112849, https://doi.org/10.1016/j.bios.2020.112849.

9. A. Amini, R. M. Guijt, T. Themelis, J. De Vos, and S. Eeltink, "Recent Developments in Digital Light Processing 3D-Printing Techniques for Microfluidic Analytical Devices," *Journal of Chromatography A* 1692 (2023): 463842, https://doi.org/10.1016/j.chroma.2023.463842.

10. S. Swetha, T. J. Sahiti, G. S. Priya, K. Harshitha, and A. Anil, "Review on Digital Light Processing (DLP) and Effect of Printing Parameters on Quality of Print," *Interactions* 245, no. 1 (2024): 178, https://doi.org/10.1007/s10751-024-02018-5.

11. J. Cheng, S. Yu, R. Wang, and Q. Ge, "Digital Light Processing Based Multimaterial 3D Printing: Challenges, Solutions and Perspectives," *International Journal of Extreme Manufacturing* 6, no. 4 (2024): 042006, https://doi.org/10.1088/2631-7990/ad4a2c.

12. A. Kausar, "Role of Thermosetting Polymer in Structural Composite," *American Journal of Polymer Science & Engineering* 5 (2017): 1–12.

13. T. Yan, A. H. Balzer, K. M. Herbert, T. H. Epps, and L. S. T. J. Korley, "Circularity in Polymers: Addressing Performance and Sustainability Challenges Using Dynamic Covalent Chemistries," *Chemical Science* 14, no. 20 (2023): 5243–5265, https://doi.org/10.1039/d3sc00551h.

14. G. Zhu, H. A. Houck, C. A. Spiegel, C. Selhuber-Unkel, Y. Hou, and E. Blasco, "Introducing Dynamic Bonds in Light-based 3D Printing," *Advanced Functional Materials* 34, no. 20 (2024): 2300456, https://doi.org/10.1002/adfm.202300456.

15. S. A. Begum, P. S. G. Krishnan, and K. Kanny, "Bio-based Polymers: A Review on Processing and 3D Printing," *Polymer Science—Series A* 65 (2023): 421–446, https://doi.org/10.1134/S0965545X2360045X.

16. V. S. D. Voet, J. Guit, and K. Loos, "Sustainable Photopolymers in 3D Printing: A Review on Biobased, Biodegradable, and Recyclable Alternatives," *Macromolecular Rapid Communications* 42, no. 3 (2021): 2000475, https://doi.org/10.1002/marc.202000475.

17. S. Rana, M. Solanki, N. G. Sahoo, and B. Krishnakumar, "Bio-Vitrimers for Sustainable Circular Bio-Economy," *Polymers* 14, no. 20 (2022): 4338, https://doi.org/10.3390/polym14204338.

18. S. Kamarulzaman, Z. M. Png, E. Q. Lim, I. Z. S. Lim, Z. Li, and S. S. Goh, "Covalent Adaptable Networks From Renewable Resources: Crosslinked Polymers for a Sustainable Future," *Chemistry (Weinheim An Der Bergstrasse, Germany)* 9, no. 10 (2023): 2771–2816, https://doi.org/10.1016/j.chempr.2023.04.024.

19. A. Kumar and L. A. Connal, "Biobased Transesterification Vitrimers," *Macromolecular Rapid Communications* 44, no. 7 (2023): 2200892, https://doi.org/10.1002/marc.202200892.

20. W. Alabiso and S. Schlögl, "The Impact of Vitrimers on the Industry of the Future: Chemistry, Properties and Sustainable Forward-looking Applications," *Polymers* 12, no. 8 (2020): 1660, https://doi.org/10.3390/POLYM12081660.

21. B. Krishnakumar, R. V. S. P. Sanka, W. H. Binder, V. Parthasarthy, S. Rana, and N. Karak, "Vitrimers: Associative Dynamic Covalent Adaptive

Networks in Thermoset Polymers," *Chemical Engineering Journal* 385 (2020): 123820, https://doi.org/10.1016/j.cej.2019.123820.

22. A. Mariani and G. Malucelli, "Biobased Vitrimers: Towards Sustainability and Circularity," *Chemical Communications* 61 (2025): 2173–2189, https://doi.org/10.1039/d4cc05967k.

23. A. Sharma, A. Chand, I. Singh, and B. Gaur, "Vitrimers for 3D Printing Technology: Current Status and Future Perspectives," *Industrial & Engineering Chemistry Research* 64, no. 5 (2025): 2491–2515, https://doi.org/10.1021/acs.iecr.4c03705.

24. V. R. Madduluri, A. Bendi, G. P. M. Chinmay, R. Roslan, and M. H. Ab Rahim, "Recent Advances in Vitrimers: A Detailed Study on the Synthesis, Properties and Applications of Bio-Vitrimers," *Journal of Polymers and the Environment* 33 (2024): 301–322, https://doi.org/10.1007/s10924-024-03416-0.

25. G. Ye, S. Huo, C. Wang, et al., "Strong yet Tough Catalyst-Free Transesterification Vitrimer With Excellent Fire-Retardancy, Durability, and Closed-Loop Recyclability," *Small* 20, no. 45 (2024): 2404634, https://doi.org/10.1002/smll.202404634.

26. M. Surós, D. Santiago, P. Verdugo, M. Pedrola, and S. De la Flor, "Reversible Adhesives From Epoxy-based Transesterification-induced Vitrimers," *Polymer (Guildf)* 299 (2024): 126939, https://doi.org/10.1016/j.polymer.2024.126939.

27. S. S. Dasari, S. M. Cotton, L. E. Arrambide, et al., "Joule Heating and Synthesis of Transesterification Vitrimer and Epoxy System," *Applied Materials Today* 44 (2025): 102705, https://doi.org/10.1016/j.apmt.2025.102705.

28. Z. Zhao, C. Qi, G. Li, et al., "Preparation and Characterization of Epoxy Vitrimer Asphalt Based on Transesterification Dynamic Covalent Bond System," *Fuel* 388 (2025): 134530, https://doi.org/10.1016/j.fuel.2025.134530.

29. R. M. Johnson, K. P. Cortés-Guzmán, S. D. Perera, et al., "Lignin-based covalent adaptable network resins for digital light projection 3D printing," *Journal of Polymer Science* 62, no. 12 (2024): 2585–2596, https://doi.org/10.1002/pol.20230026.

30. S. Grauzeliene, A. S. Schuller, C. Delaite, and J. Ostrauskaite, "Biobased Vitrimer Synthesized From 2-hydroxy-3-phenoxypropyl Acrylate, Tetrahydrofurfuryl Methacrylate and Acrylated Epoxidized Soybean Oil for Digital Light Processing 3D Printing," *European Polymer Journal* 198 (2023): 112424, https://doi.org/10.1016/j.eurpolymj.2023.112424.

31. G. N. Kamble and A. Sk, "Biobased Reprintable Bis-Dynamic Covalent Photopolymer Composition for Digital Light Processing 3D Printing With Self-Healing Properties," *ACS Applied Polymer Materials* 7 (2025): 1401–1410, https://doi.org/10.1021/acsapm.4c03116.

32. M. C. Cabua, M. V. Piras, and D. Dessi, "Microcrystalline Cellulose From Aloe Plant Waste as a Platform for Green Materials: Preparation, Chemical Functionalization, and Application in 3D Printing," *ACS Applied Polymer Materials* 6, no. 12 (2024): 6926–6936, https://doi.org/10.1021/acsapm.4c00409.

33. E. Rossegger, R. Höller, D. Reisinger, et al., "High Resolution Additive Manufacturing With Acrylate Based Vitrimers Using Organic Phosphates as Transesterification Catalyst," *Polymer* 221 (2021): 123631, https://doi.org/10.1016/j.polymer.2021.123631.

34. M. M. Ibrahim, W. K. El-Zawawy, Y. Jüttke, A. Koschella, and T. Heinze, "Cellulose and Microcrystalline Cellulose From Rice Straw and Banana Plant Waste: Preparation and Characterization," *Cellulose* 20, no. 5 (2013): 2403–2416, https://doi.org/10.1007/s10570-013-9992-5.

35. Y. Zhang, H. Wang, X. Sun, Y. Wang, and Z. Liu, "Separation and Characterization of Biomass Components (Cellulose, Hemicellulose, and Lignin) From Corn Stalk," *Bioresources* 16 (2021): 7205–7219, https://doi.org/10.15376/biores.16.4.7205-7219.

36. R. Javier-Astete, J. Jimenez-Davalos, and G. Zolla, "Determination of Hemicellulose, Cellulose, Holocellulose and Lignin Content Using FTIR in Calycophyllum Spruceanum (Benth.) K. Schum. And Guazuma crinita Lam," *PLoS ONE* 16, no. 10 (2021): 0256559, https://doi.org/10.1371/journal.pone.0256559.

37. F. D. Zhang, C. H. Xu, M. Y. Li, X. D. Chen, Q. Zhou, and A. M. Huang, "Identification of Dalbergia Cochinchinensis (CITES Appendix II) From Other Three Dalbergia Species Using FT-IR and 2D Correlation IR Spectroscopy," *Wood Science and Technology* 50, no. 4 (2016): 693–704, https://doi.org/10.1007/s00226-016-0815-3.

38. S. Cichosz, A. Masek, and K. Dems-Rudnicka, "Original Study on Mathematical Models for Analysis of Cellulose Water Content From Absorbance/Wavenumber Shifts in ATR FT-IR Spectrum," *Scientific Reports* 12, no. 1 (2022): 19739, https://doi.org/10.1038/s41598-022-24097-6.

39. S. Park, J. O. Baker, M. E. Himmel, P. A. Parilla, and D. K. Johnson, "Cellulose Crystallinity Index: Measurement Techniques and Their Impact on Interpreting Cellulase Performance," *Biotechnology for Biofuels* 3, no. 1 (2010): 10, https://doi.org/10.1186/1754-6834-3-10.

40. M. Bifano, "Digital Light Processing: A Review on the Printing Resolution and the Materials Options," *Applied and Computational Engineering* 1 (2022): 17–25, https://doi.org/10.54254/ace.2022002.

41. M. Ghaemy, M. Heidaripour, and M. Barghamadi, "Synthesis, Characterization, and Cure Reaction of Methacrylate-Based Multifunctional Monomers for Dental Composites," *Journal of Applied Polymer Science* 106, no. 3 (2007): 1917–1923, https://doi.org/10.1002/app.26899.

42. N. Goswami, C. Laukamp, and B. Pejcic, "Infrared Spectroscopic Study of Vibration Modes in Th-bearing, Multi-2 REE Natural Monazites," *Spectrochimica Acta Part A, Molecular and Biomolecular Spectroscopy* 344 (2025): 126603, https://doi.org/10.1016/j.saa.2025.126603.

43. I. Niskanen, K. Zhang, M. Karzarjeddi, et al., "Optical Properties of Cellulose Nanofibre Films at High Temperatures," *Journal of Polymer Research* 29, no. 5 (2022): 187, https://doi.org/10.1007/s10965-022-03019-0.

44. A. Romano, O. Konuray, F. Román, et al., "Critical Analysis of the Thermal Stability of Transesterification Vitrimers for 3D -Printing Applications Based on Digital Light Processing," *Polymer International* 73, no. 4 (2024): 280–286, https://doi.org/10.1002/pi.6592.

Supporting Information

Additional supporting information can be found online in the Supporting Information section.

Supporting File: mame70190-sup-0001-SuppMat.docx.